

# SAGD: Boundary-Enhanced Segment Anything in 3D Gaussian via Gaussian Decomposition

Xu Hu<sup>1,2</sup> Yuxi Wang<sup>2,3</sup> Lue Fan<sup>3,4</sup> Junsong Fan<sup>2,3</sup> Junran Peng<sup>3,5</sup>  
Zhen Lei<sup>2,3,4</sup> Qing Li<sup>1†</sup> Zhaoxiang Zhang<sup>2,3,4†</sup>

<sup>1</sup>The Hong Kong Polytechnic University <sup>2</sup>Center for Artificial Intelligence and Robotics, HKISI, CAS

<sup>3</sup>Institute of Automation, Chinese Academy of Sciences

<sup>4</sup>University of Chinese Academy of Sciences <sup>5</sup>Chongyue Technology

**Abstract.** 3D Gaussian Splatting has emerged as an alternative 3D representation for novel view synthesis, benefiting from its high-quality rendering results and real-time rendering speed. However, the 3D Gaussians learned by 3D-GS have ambiguous structures without any geometry constraints. This inherent issue in 3D-GS leads to a rough boundary when segmenting individual objects. To remedy these problems, we propose SAGD, a conceptually simple yet effective boundary-enhanced segmentation pipeline for 3D-GS to improve segmentation accuracy while preserving segmentation speed. Specifically, we introduce a Gaussian Decomposition scheme, which ingeniously utilizes the special structure of 3D Gaussian, finds out, and then decomposes the boundary Gaussians. Moreover, to achieve fast interactive 3D segmentation, we introduce a novel training-free pipeline by lifting a 2D foundation model to 3D-GS. Extensive experiments demonstrate that our approach achieves high-quality 3D segmentation without rough boundary issues, which can be easily applied to other scene editing tasks. Our code is public available at <https://github.com/XuHu0529/SAGS>.

**Keywords:** 3D Gaussian Splatting · 3D Segmentation · Boundary Issues

## 1 Introduction

3D scene understanding is a challenging and crucial task in computer vision and computer graphics, which involves scene reconstruction from images or videos and the perception of a given 3D real-world environment. Researchers have conducted extensive studies in scene reconstruction and 3D scene perception in recent years. For instance, Neural Radiance Fields (NeRF) [5, 11, 21, 30] have significantly contributed to the progress of 3D scene reconstruction by representing scenes in an implicit way. In the field of scene perception, continuous research is being conducted on 3D detection and semantic segmentation, based on the representation of range images [8, 20], point clouds [7, 10, 15, 26, 29], and Bird’s

---

<sup>†</sup>Corresponding author.

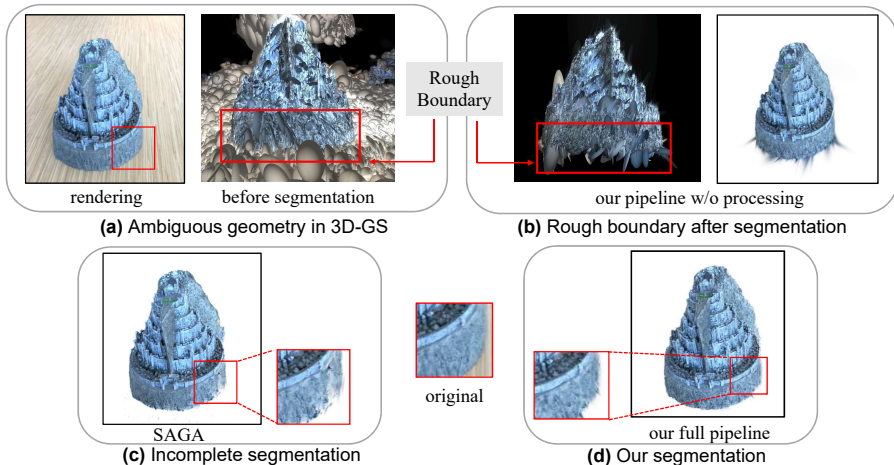


**Fig. 1:** (a) The training of 3D-GS doesn't consider the structure of objects, leading to the ambiguous geometry; (b) Direct segmentation without Gaussian Decomposition processing will result in rough boundary segmentation; (3) The recent SAGA also has incomplete segmentation caused by the same issue; (d) Our full pipeline considers this issue and can achieve better segmentation.

Eye View (BEV) [17, 24, 25, 27, 33]. Although current methods have attained noteworthy success in 3D scene understanding, the time-consuming nature of NeRF and the high costs associated with 3D data collection pose challenges for scaling up these approaches.

Recently, 3D Gaussian Splatting (3D-GS) [12] is emerging as a prospective method for modeling static 3D scenes. 3D-GS characterizes intricate scenes by employing numerous colored 3D Gaussians, rendering them into camera views through splatting-based rasterization. Through differentiable rendering and gradient-based optimization, the positions, sizes, rotations, colors, and opacities of these Gaussians can be finely tuned to accurately represent the 3D scene, availing for the comprehension of a 3D environment. Segmentation in 3D-GS is quite a natural pathway to scene understanding for its explicit representation. Recent works [3, 16, 34, 37] have been proposed to achieve segmentation in 3D-GS via lifting 2D foundation models in a learnable way. They share the same ideas to distill other features or identity encodings generated from 2D foundation models to 3D Gaussian fields.

However, the Gaussians learned by 3D-GS are ambiguous without any geometry constraint, leading to the issue of boundary roughness. A single Gaussian might correspond to multiple objects, complicating the task of accurately segmenting individual objects (shown in Fig. 1 (a)). As shown in Fig. 1 (b), direct segmentation will leave rough edges at the boundary. This is because these Gaussians across multiple objects will be left if no additional processing is performed. In addition, even if SAGA [3] uses filtering and growing post-processing for seg-

mented 3D Gaussians, its feature matching method also has the limitation of incomplete boundary, as shown in Fig. 1 (c).

We present our boundary-enhanced segmentation method, an interactive training-free pipeline for efficient and effective segmentation in 3D-GS without rough boundary issues. By leveraging the 2D foundation model SAM [14], our method can generate a segmented mask from a single input view based on the given prompts. Starting from the obtained mask, our method automatically generates multi-view masks and achieves consistent 3D segmentation via the proposed assignment strategy. Specifically, to resolve the inherent boundary issues, we incorporate a simple but effective Gaussian Decomposition scheme, ingeniously utilizing the special structure of 3D Gaussian. Since the boundary roughness issue results from the non-negligible spatial sizes of 3D Gaussians located at the boundary, our key insight is to find and then decompose the original boundary Gaussians according to our proposed principles. Consequently, our method eliminates the inherent issues and achieves more complete segmentation quickly and efficiently, as shown in Fig. 1 (d).

In summary, the contributions of this paper are as follows:

- We propose a simple yet effective training-free pipeline for segmentation in 3D Gaussians without any learnable parameters;
- We incorporate the Gaussian Decomposition module to mitigate the boundary roughness issues in 3D segmentation resulting from inherent 3D-GS geometry;
- Extensive segmentation experiments on a considerable amount of 3D scenes and editing applications demonstrate the effectiveness of our proposed method.

## 2 Related Work

### 2.1 3D Gaussian Splitting

3D Gaussian Splatting [12] is a technique for scene reconstruction, which has been shown to be an alternative 3D representation as NeRF, benefiting from both its high-quality rendering results and real-time rendering speed. Recent research on this technique contains applying 3D Gaussian in dynamic scene and combining it with diffusion model to achieve 3D generation. Dynamic 3D Gaussians [19] extends Gaussian Splatting to dynamic scenes via tracking 3D objects modeled as a set of 3D Gaussians. DreamGaussian [31], GaussianDreamer [35] and GSGEN [6] combine 3D Gaussians with diffusion models to generate high-quality 3D assets.

### 2.2 Segmentation in Radiance Fields

Neural Radiance Fields (NeRFs) are a popular way of representing 3D scenes implicitly with neural networks. Many researchers have explored how to segment objects in 3D using NeRFs, for various applications such as novel view synthesis, semantic segmentation, 3D inpainting, and language grounding. Some methods,

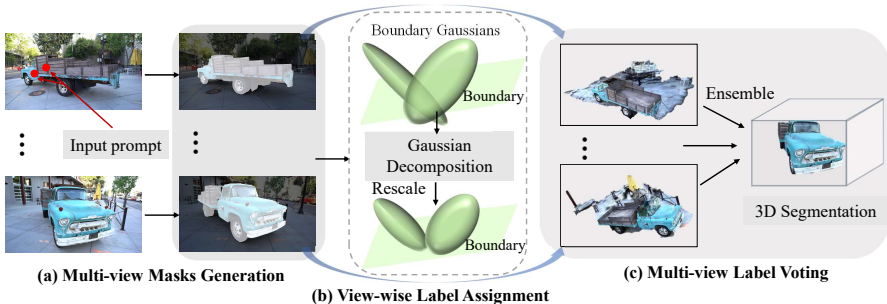


**Fig. 2:** Pipeline of our proposed method. (a) Given a set of clicked points on the 1<sup>st</sup> rendered view, we utilize SAM to generate masks for corresponding objects under every view automatically; (b) For every view, Gaussian Decomposition is first performed to address the issue of boundary roughness and then label propagation is implemented to assign binary labels to each 3D Gaussian; (c) Finally, with assigned 3D labels from all views, we adopt a simple yet effective voting strategy to determine the segmented Gaussians.

such as Semantic-NeRF [36], NVOS [28], and SA3D [4], use different types of inputs to guide the segmentation, such as semantic labels, user scribbles, or 2D masks. Other methods, such as N3F [32], DFF [32], LERF [13], and ISRF [9], learn additional feature fields that are aligned with NeRFs, and use 2D visual features from pre-trained models or language embeddings to query the 3D features. These methods usually require modifying or retraining the original NeRF models or training other specific parameters to obtain the 3D segmentation. However, limited by the representation and rendering speed of NeRF, it is challenging to apply it to more practical applications, such as scene editing, collision analysis, etc. Inspired by the real-time 3D-GS, recent works [3, 16, 34, 37] have been proposed to achieve segmentation in 3D-GS in a learnable way. SAGA [3] and Featue 3DGS [37] distill the knowledge embedded in the SAM decoder into the feature field of 3D-GS, and Gaussian-Grouping [34] supervises the Identity Encodings during the differentiable rendering by leveraging the 2D mask predictions by SAM. However, no research has been proposed to solve the rough boundary issues in segmentation resulting from the inherent properties of 3D Gaussians. In this work, we are the first to propose a novel Gaussian Decomposition scheme to solve this issue, incorporated into our effective training-free segmentation pipeline.

### 3 Method

In this section, we first present the preliminary in 3D Gaussian Splatting in Sec. 3.1 for clear understanding and then define the problem and task in Sec. 3.2. Our basic training-free pipeline consists of Sec. 3.3 and Sec. 3.5. The details of Gaussian Decomposition are described in Sec. 3.4. The pipeline of our method can be seen in Fig. 2.



### 3.1 Preliminary: 3D Gaussian Splatting

3D Gaussian Splatting (3D GS) [12] is an emerging method for real-time radiance field rendering. It has been proven effective in Novel View Synthesis with high rendering quality as NeRF and real-time rendering speed. 3D GS represents scenes with a set of 3D Gaussians. Specifically, each 3D Gaussian is parameterized by a position  $\mu \in \mathbb{R}^3$ , a covariance matrix  $\Sigma$ , an opacity value  $\alpha$ , and spherical harmonics (SH).

To render an image, it uses the splatting rendering pipeline, where 3D Gaussians are projected onto the 2D image plane. The projection transforms 3D Gaussians into 2D Gaussians in the image plane. All 2D Gaussians are blended together by the  $\alpha$ -blending algorithm to generate the color:

$$\mathbf{c} = \sum_{i \in N} \mathbf{c}_i \alpha_i \prod_{j=1}^{i-1} (1 - \alpha_j), \quad (1)$$

During the  $\alpha$ -blending process, for each 2D Gaussian, only the 2D points with probability density larger than a certain threshold are calculated. This means a 2D Gaussian and 3D Gaussian can be intuitively regarded as a 2D **ellipse** and a 3D **ellipsoid** respectively. Empirically, for an axis of the ellipse, its length is set to  $3\sigma$ , where  $\sigma$  is the square root of the variance in the axis.

### 3.2 Problem Definition

Given a set of trained 3D gaussians  $\mathbb{G} = \{\mathbf{g}_0, \mathbf{g}_1, \dots, \mathbf{g}_n\}$  and a random initial view  $\mathbf{v}_0$ , users could offer 2D point prompt set  $\mathbb{P}_{2D} = \{\mathbf{p}_0, \mathbf{p}_1, \dots, \mathbf{p}_m\}$  to specify a 2D object in view  $\mathbf{v}_0$ . Our algorithm is supposed to segment the corresponding 3D object  $\mathbb{O}$  in  $\mathbb{G}$  according to the human prompts, where  $\mathbb{O}$  is a subset of  $\mathbb{G}$ .

Let  $\mathbf{m}_i$  denote the projected binary mask of  $\mathbb{O}$  in  $i$ -th view, an accurate segmentation  $\mathbb{O}$  means  $\mathbf{m}_i$  equals to  $\mathbf{m}_i^*$  for  $\forall i \in \{0, 1, \dots, n\}$ . Here  $\mathbf{m}_i^*$  is the ground truth mask of  $\mathbb{O}$  in  $i$ -th view. Different from the conventional 2D segmentation mask in the image or 3D segmentation task in the point cloud, there is no ground truth for 3D Gaussians. Thus, our algorithm is designed to minimize the difference between  $\mathbf{m}_i$  and  $\mathbf{m}_i^*$ .

### 3.3 Segment 3D Gaussians with 2D Mask

**3D Prompts for Multiview Masks Generation.** By the definition in Sec. 3.2, users are given the first rendered view to specify the target object. However, only the first view is far from sufficient to segment the target object in 3D space. So here we first generate multiview masks to aid the 3D segmentation. With multiple masks from different views, a 3D object can be segmented by the intersection of the corresponding frustum of these masks.

The core of obtaining masks is to generate 2D prompt points in each view. Denoting the  $i$ -th 2D prompt point in the first given view  $\mathbf{v}_0$  as  $\mathbf{p}_i^0$ , we define

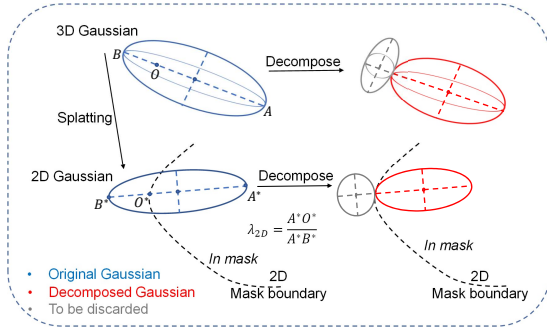


**Fig. 3:** Illustration of the Gaussian Decomposition process.

the corresponding 3D prompt  $\mathbf{p}_i^{3D}$  as:

$$\arg \min_{\mu} \{d(\mu), d(\mu) > 0 \mid \mu \in \mathbb{G}, \|\mathbf{P}_0\mu - \mathbf{p}_i^0\|_1 < \epsilon\}, \quad (2)$$

where  $d(\mu)$  is the depth of Gaussian center  $\mu$  and  $\mathbf{P}_0$  is the projection for initial view  $\mathbf{v}_0$ . Thus  $\mathbf{P}_0\mu$  is the position of  $\mu$  in view  $\mathbf{v}_0$ . Eq. 2 indicates that the corresponding 3D prompt of  $\mathbf{p}_i$  is the center of a certain 3D Gaussian. This center meets two requirements: (1) it has a similar projected position with  $\mathbf{p}_i$  with a Manhattan distance less than  $\epsilon$ , and (2) if there are multiple 3D Gaussian centers satisfying the first requirement, the one with the smallest positive depth is selected as the 3D prompt.

For all the 2D prompt points in the first view, we could get a set of 3D prompt by Eq. 2. Then for another view  $\mathbf{v}_i$ , we project these 3D prompts into the 2D plane, resulting in 2D prompts in the view  $\mathbf{v}_i$ . In this way, we obtain 2D prompts in all views, and all masks are obtained by prompting the SAM.

**View-wise Label Assignment.** With all the masks, we proceed to assign binary labels to each 3D Gaussian. In particular, we maintain a matrix  $\mathbf{L}$ , whose element  $\mathbf{L}_{ij}$  is defined by

$$\mathbf{L}_{ij} = \begin{cases} 1 & \text{if } \mathbf{P}_j\mu_i \in \mathbf{m}_j, \\ 0 & \text{if } \mathbf{P}_j\mu_i \notin \mathbf{m}_j, \end{cases} \quad (3)$$

where  $\mu_i$  is the  $i$ -th Gaussian center of the scene and  $\mathbf{m}_j$  is the foreground mask in  $j$ -th view.  $\mathbf{P}_j$  stands for the projection matrix of  $j$ -th view.

### 3.4 Gaussian Decomposition

After obtaining the prompt points of each view, we could assign labels to 3D Gaussians by the projected position of its center. However, 3D Gaussian has non-negligible spatial volume, so those Gaussians projected to the mask boundary usually have a part out of the boundary, greatly increasing the roughness of boundaries. A straightforward solution is directly removing the Gaussians across

mask boundaries. However, such a solution greatly damages the 3D structures of the object.

To address this issue, we propose the *Gaussian Decomposition* to mitigate the boundary roughness while maintaining the 3D structures as complete as possible. Fig. 3 illustrates the basic idea of Gaussian decomposition. It has two basic steps to achieve the Gaussian decomposition: **(1)** For each 3D Gaussian, we obtain the corresponding 2D Gaussian by projection and mark it as a boundary Gaussian if one of its long-axis endpoints is outside of the 2D mask. Then, as shown in Fig. 3, we denote the two ends of the long axis of a 2D Gaussian as  $A^*$  and  $B^*$ , and the intersection of  $A^*B^*$  and mask boundary is  $O^*$ .  $A$ ,  $B$ , and  $O$  are the corresponding 3D points in the long axis of the 3D Gaussian. Assuming  $A^*$  is in the mask while  $B^*$  is out of the mask, we define

$$\lambda_{3D} = \frac{OA}{AB}, \quad (4)$$

$$\lambda_{2D} = \frac{O^*A^*}{A^*B^*}. \quad (5)$$

**(2)** After obtaining the boundary Gaussians, we solve the ratio  $\lambda_{3D}$  by first calculating  $\lambda_{2D}$  and then decompose the original 3D Gaussian according to  $\lambda_{3D}$ .

However, the transformation from  $\lambda_{2D}$  to  $\lambda_{3D}$  is not straightforward because the perspective projection from 3D space to 2D space is not affine, which means the ratios are different. Fortunately, 3D Gaussian Splatting leverages local affine approximation to simplify the rendering process. It projects 3D Gaussian to the 2D plane by

$$\Sigma' = JW\Sigma W^T J^T \quad (6)$$

where  $\Sigma$ ,  $\Sigma'$  are the covariance matrix of the 3D and 2D gaussian distribution, respectively.  $W$  is the projection transformation and  $J$  is the Jacobian of affine approximation derived in EWA algorithm [38]. Eq. 6 indicates that Gaussian Splatting simplifies the perspective projection to an affine projection, thus decomposition scaling ratio  $\lambda_{3D}$  in 3D space is equivalent to the ratio  $\lambda_{2D}$  in the 2D plane.

Let  $\mathbf{g}$  denote a 3D Gaussian across the boundary. Its scale in the long axis and the 3D center are defined as  $s$  and  $\mu$ , respectively. We have

$$s' = \lambda_{2D}s, \quad (7)$$

$$\mu' = \mu + \frac{1}{2}(s - \lambda_{2D}s)\mathbf{e}, \quad (8)$$

where  $\mathbf{e}$  is the unit vector pointing from the 3D Gaussian center to the in-mask endpoint of the long axis. The decomposed Gaussian  $\mathbf{g}'$  adopt  $\mu'$  and  $s'$  as the new center and long-axis scale, maintaining other properties unchanged. Another decomposed Gaussian outside of the mask is removed.

### 3.5 Multiview Label Voting

So far, every 3D Gaussian including the decomposed one has a list of binary labels  $\mathbf{L}_i$ , using the label assignment in Sec. 3.3. Leveraging the assigned labels,

**Table 1:** Quantitative results on SPIn-NeRF dataset. ‘‘Singe view’’ denotes projecting the 2D segmentation result to 3D simply, thus we don’t consider its time cost. There is extra time cost (about 10mins) for SAGA to distill 2D knowledge to 3D-GS, while other methods don’t need this process.

Scenes	Single View [4]		MVSeg [23]		SA3D [4]		SAGA [3]		Ours	
	IoU	Acc	IoU	Acc	IoU	Acc	IoU	Acc	IoU	Acc
Orchids	79.4	96.0	92.7	98.8	83.6	96.9	-	-	85.4	97.5
Ferns	95.2	99.3	94.3	99.2	97.1	99.6	-	-	92.0	98.9
Room	73.4	96.5	95.6	99.4	88.2	98.3	-	-	86.5	98.1
Horns	85.3	97.1	92.8	98.7	94.5	99.0	-	-	91.1	98.4
Fortress	94.1	99.1	97.7	99.7	98.3	99.8	-	-	96.6	99.5
Fork	69.4	98.5	87.9	99.5	89.4	99.6	-	-	83.4	99.3
Pinecone	57.0	92.5	93.4	99.2	92.9	99.1	-	-	92.0	99.0
Truck	37.9	77.9	85.2	95.1	90.8	96.7	-	-	93.0	97.9
Lego	76.0	99.1	74.9	99.2	92.2	99.8	-	-	88.4	99.7
Mean	74.1	95.2	90.5	98.8	91.9	98.8	88.0	98.5	89.9	98.7
Time cost (/object)	-		3-6mins		2-10mins		0.08s-0.9s (+10mins)		within 15s	

here we adopt a simple yet effective heuristic rule to determine if a 3D Gaussian  $g_i$  belongs to the target 3D object. In particular, we first define the confidence score  $s_i$  of  $g_i$  as

$$s_i = \frac{1}{N} \sum_{j=0}^{N-1} L_{ij}, \quad (9)$$

where  $N$  is the number of views. Then we adopt a threshold  $\tau$  and regard a Gaussian with a score higher than  $\tau$  as positive.

## 4 Experiments

### 4.1 Datasets

We choose different datasets to testify our method, including LLFF [22], Mip-NeRF 360 [2], LERF [13], and some test scenes from the 3D Gaussian Splatting [12]. These datasets contain both small indoor objects and large outdoor scenes, which are very complex and challenging. For quantitative experiments, because there is no existing benchmark that can be used in 3D Gaussian space, we use the SPIn-NeRF [23] dataset with 2D ground-truth for evaluation.

### 4.2 Quantitative results

We first conduct experiments on the SPIn-NeRF [23] dataset for quantitative analysis. Given a set of images of the scene, we follow the process described in

**Table 2:** Quantitative results with text prompts on four scenes of SPIn-NeRF dataset.

Scene	room	truck	fortress	pinecone
Text	“the table”	“the truck”	“the fortress”	“the pinecone”
IoU	86.3	93.7	92.8	86.5
Acc	97.9	97.8	98.8	97.0

Section 3 to obtain the segmentation of the target object in 3D Gaussian Space. The segmented 3D Gaussians are used to render 2D masks in other views. Finally, we calculate the IoU and Accuracy between these rendered and the ground-truth masks. Results can be seen in Table 1.

In the comparison, it is noteworthy that both the MVSeg [23] and the SA3D [4] require additional parameters and a computation-costly training process. While SAGA [3] shows nearly one-thousandth of the time compared with them, it needs extra training time (10 minutes per scene) to distill the knowledge embedded in the SAM decoder into the feature field. By contrast, the “Single view” [4] refers to mapping the 2D masks to the 3D space based on the corresponding depth information, which does not need additional training process. In this sense, our method is the same as the “Single view” that does not incorporate any additional training or model parameters. Results show that our approach can achieve comparable segmentation quality to the MVSeg and SA3D methods and better results than SAGA. The time cost of ours is much less than MVSeg and SA3D. Considering the training time of SAGA, the average segmentation cost of a single object is basically the same as our method. In some 360 outdoor scenes, such as “Truck”, our approach even outperforms the SA3D and the MVSeg. When compared with the training-free method “Single view”, our approach achieves a significant promotion of +15.8% IoU and +3.5% Acc. These results demonstrate our approach is very efficient in obtaining high-quality segmentation masks.

Next, we replace the above point prompts with text prompts corresponding to the objects. Given a text input, we prompt the Grounding DINO [18] to generate target bounding boxes, which serve as input prompts for the SAM to obtain 2D segmentation masks. Then, following the segmentation process in Section 3, we can transform the 2D masks into 3D Gaussian masks corresponding to the text input. Similar to the above evaluation process, we also calculate the IoU and Acc between 2D rendered masks and given ground-truth masks. Quantitative results are shown in Table 2. For both room and truck scenes, the IoU and Acc values can achieve a similar level as using clicked points as input prompts. These results demonstrate our method can combine multi-modal prompts as input.

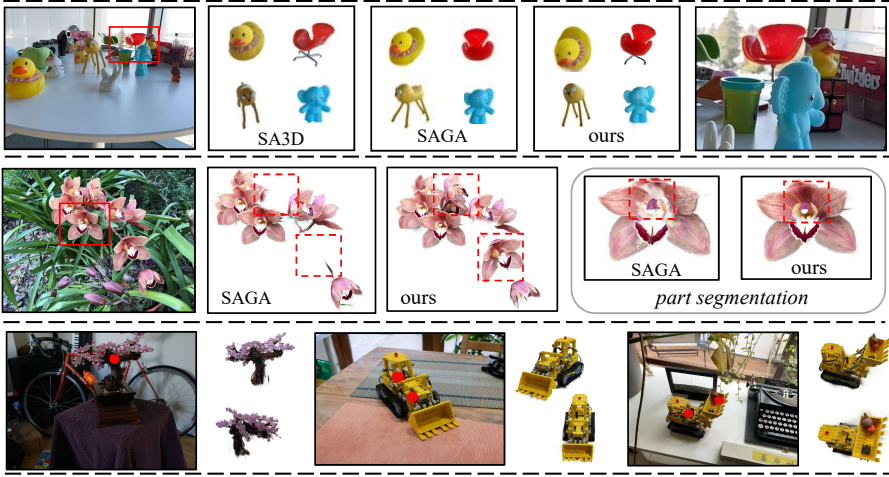


**Fig. 4:** Qualitative results compared with SA3D [4] and SAGA [3] in different scenes (LERF-figurines [13], SPIn-NeRF-Orchids [23], LERF-dozer-nerfgun-waldo [13]). We enlarge the boxed area on the right for a better visualization.

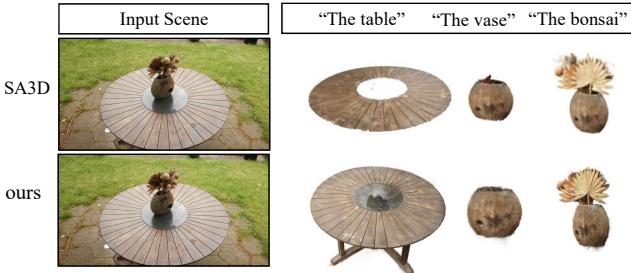


**Fig. 5:** 3D segmentation results with text prompts in Mip-NeRF360-garden [2].

### 4.3 Qualitative results

We conduct four kinds of tasks to demonstrate the potential application and qualitative performance of our approach, including point-guided segmentation, text-guided segmentation, scene editing, and collision detection.

**Point-Guided Segmentation:** We first conduct visualization experiments on 3D object segmentation guided by one or a set of point prompts clicked on the first-view rendered image. The results are shown in Fig. 4. The first row shows the segmentation results of SA3D, SAGA and ours on LERF-figurines scene. The second row compares with SAGA, which distills the knowledge embedded in the SAM decoder into the feature field. Though the boundary issues in 3D-GS can be alleviated, incomplete segmentation occurs even after post-processing. In contrast, ours can solve the boundary problems while achieving more complete segmentation. More segmentation results are shown in the third row.

**Text-Guided Segmentation:** We further conduct 3D object segmentation experiments guided by text prompts. We follow the same process as in Table 2 ex-

**Table 3:** Ablation on Gaussian decomposition (GD) on SPIn-NeRF dataset. The 2nd and 3rd columns compare the results before and after using the Gaussian decomposition (GD). The last column represents the results of directly removing the gaussians across mask boundaries.

Scene	w/ GD		w/o GD		Delete	
	IoU	Acc	IoU	Acc	IoU	Acc
Orchids	85.4	97.5	82.2	96.8	78.2	95.4
Ferns	92.0	98.9	89.2	98.4	89.8	98.5
Room	86.5	98.1	81.3	97.2	85.4	97.9
Horns	91.1	98.4	83.2	96.5	84.8	97.6
Fortress	96.5	99.4	88.5	98.1	82.3	96.7
Fork	83.4	99.3	81.8	99.2	79.9	99.1
Pinecone	92.1	98.9	91.6	98.9	82.9	97.5
Truck	94.0	97.9	93.4	97.8	91.4	96.8
Lego	88.4	99.7	88.4	99.6	82.9	99.4
mean	<b>89.9</b>	98.7	86.6	98.1	84.2	97.7

periments to conduct visualization experiments. In order to compare our method with SA3D under the same setting, we choose the same garden scene from Mip-NeRF 360 dataset [2], using three text prompts including “The table”, “The vase” and “The bonsai”. Results in Fig. 5 show that our approach can achieve accurate segmentation results by simply providing object names, demonstrating our method’s potential in combining with language models. Compared with the SA3D in the “The table” case, our approach can segment the complete object with desired table legs, while SA3D only gives the tabletop.

**Comparison between 2D and 3D Segmentation:** Our method improves the segmentation quality of SAM. Due to the sensitivity of SAM to the scene viewpoint, the 2D segmentation results might be incomplete under some views, but our 3D segmentation can still guarantee complete segmentation results via a multi-view ensemble (Fig. 6).

**Scene Editing:** Scene editing is a basic application for 3D reconstructed scenes. However, it’s quite difficult to do this without being able to locate the specific objects. This task demonstrates the ability of our approach to help edit the 3D scenes. Specifically, after segmenting the objects in the 3D Gaussian space, we can manipulate the objects by removing, translating, and rotating them. Thanks to the simplicity of the explicit Gaussian representations, without bells and whistles, our approach obtains satisfactory scene editing results, as shown in Fig. 7. The instances in 1st column with red bounding boxes are objects to be segmented. It can be seen that with objects segmented in 3D Gaussians, they can be translated and rotated in any direction in the scene. After the removal of segmented objects, original scenes can still keep intact.

**Collision Detection:** Collision detection is an indispensable component in practical 3D applications, such as games, movies, and simulators. In this task, we demonstrate our approach can directly help in revealing the collision body



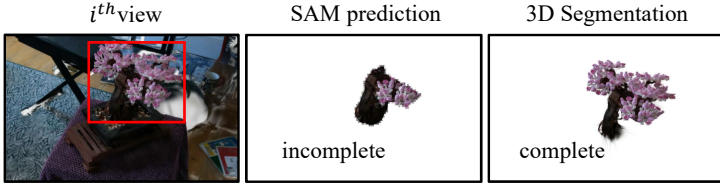


Fig. 6: Comparison between 2D and 3D Segmentation.

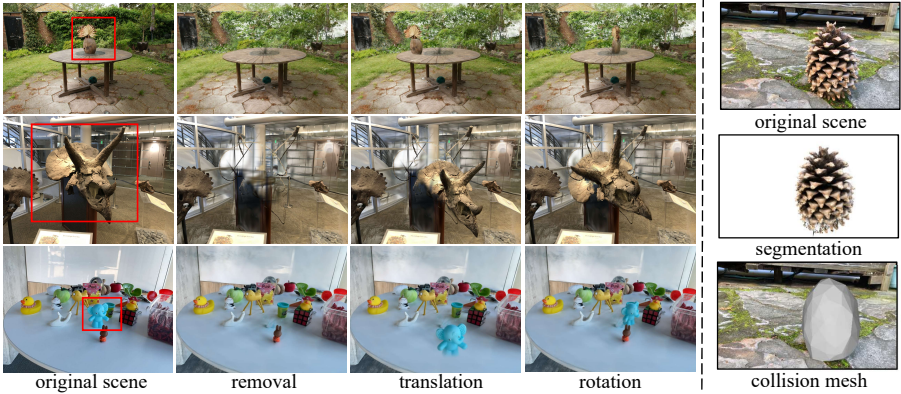


Fig. 7: Visualization examples of scene editing after the object segmentation. We offer three scene editing examples: removal, translation, and rotation. We further provide collision mesh computed after segmentation, as shown in the last column.

of target objects in the 3D Gaussian space. We choose two scenes from SPIn-NeRF dataset. Following the process of our segmentation method, we can obtain the corresponding segmented 3D Gaussian points in the scene. To this end, we use the Quickhull [1] algorithm to build the collision mesh upon our segmented objects. The results in the last column of Fig. 7 show that our segmented objects can successfully derive correct convex hulls for downstream applications.

#### 4.4 Ablation Study

**Gaussian Decomposition:** Gaussian Decomposition is proposed to address the issue of roughness boundaries of 3D segmented objects, which results from the non-negligible spatial sizes of 3D Gaussian located at the boundary. We conduct both quantitative and qualitative experiments to verify the effectiveness of our approach. For quantitative ablation experiments, Table 3 shows the results. We compare our proposed Gaussian Decomposition scheme with two other processing methods, one for segmentation without any special handling (the 3rd column), and the other for directly removing such Gaussians (the last column). The experiments are conducted on SPIn-NeRF dataset, following the same evaluation process as Table 1. Compared with the others, our proposed approach outperforms them on all scenes with +3.3% and +5.7% IoU, respectively, demonstrating the effectiveness of Gaussian Decomposition. Besides, it can be seen

**Table 4:** Ablation on different number of views for 3D segmentation. Numbers in parentheses represent the used view percentage of the total training view.

Number of views	5(10%)	10(20%)	21(50%)	42(100%)
IoU on Fortress	91.16	92.11	93.82	96.55
Number of views	25(10%)	50(20%)	125(50%)	251(100%)
IoU on truck	90.27	90.97	92.11	93.48

**Table 5:** Ablation on confidence score threshold  $\tau$  on the “truck” scene.

$\tau$	0.3	0.5	0.6	0.7	0.9
IoU	61.7	82.7	<b>93.4</b>	90.6	53.9

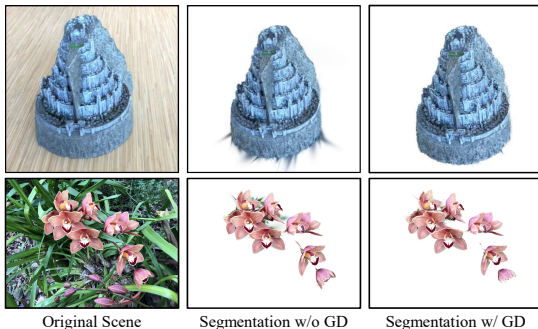
that directly removing these gaussians cannot decrease the roughness of mask boundaries, leading to even 2.4% lower IoU values.

Fig. 8 shows the visualization results for comparison. We select two representative scenes in which the junction/contact exists large-scale Gaussian points (can be seen in the 2nd column). This issue is alleviated after utilizing the proposed Gaussian Decomposition strategy. Though this idea is simple, the improvement is obvious.

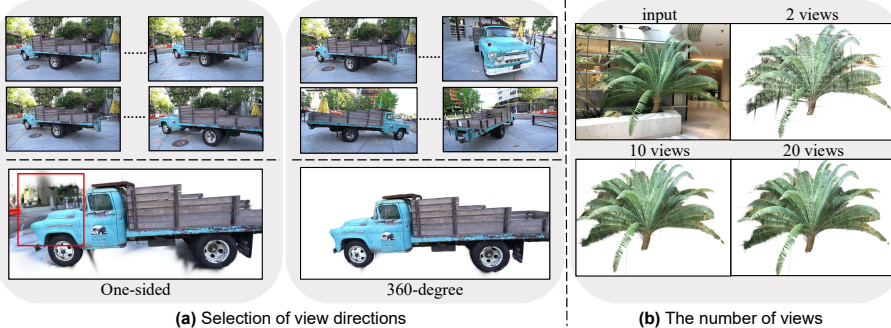
**Selection of Views:** In this section, we study the influence of selected 2D views on 3D Gaussian segmentation. Fig. 9 (b) demonstrates the segmentation quality using different numbers of views. It is noteworthy that the leaves in the “fern” scene are very tiny and challenging. Even so, with only two sparse views, our approach can achieve decent results, and the segmentation quality quickly improves when increasing the number of views. Table 4 also draws a similar conclusion: as the number of views increases, the IoU values will also increase. It is worth noting that even with sparse views (10% percentage), we can obtain relatively decent results for both two types of scenes, which also demonstrates the robustness and effectiveness of our approach. In practical applications, using sparse views (below 10% of total views) will greatly improve efficiency, although under 100% views, our method can still be completed within one minute.

Fig. 9 (a) study the influence of view directions on final segmentation results. We choose the truck with 360-degree views. The upper row shows the result of using roughly a single direction. In this case, the background is mistakenly incorporated into the segmentation. By contrast, with the same number of views but variant directions, the approach achieves high-quality clean segmentation results. This result reveals the importance of choosing non-monotone view directions in practice usage with 360 scenes.

**Hyper-Parameters:** In the process of our method, we set a hyper-parameter  $\tau$  to control the threshold of label confidence score in Sec. 3.5. As shown in Table 5, too large  $\tau$  values will lead to the partially missing the segmented objects, and too small  $\tau$  values will remain more background objects. For scenes



**Fig. 8:** Ablation results on Gaussian Decomposition (GD) on the LERF-pinecone.



**Fig. 9:** Ablation on view selection.

with some views that may cover only part of the objects to be segmented (i.e. half of the truck body in the “truck” scene), a small  $\tau$  value is preferred. In the interactive segmentation process, this threshold can be set manually according to the complexity of the scenes and the quality of camera views.

## 5 Discussions and Limitations

Through experiments, we found that our method does not perform well in objects where 3D Gaussians are very sparse, such as the LLFF-room [22] scene. The Gaussians of the table are notably sparse; even worse, the Gaussians representing the table surface are across different objects. Though our Gaussian Decomposition can somewhat remedy the boundary issue, it still suffers from extremely sparse points and leaves holes in 3D segmentation. We believe this limitation can be alleviated by future research in a more structured 3D-GS representation, yielding more accurate results.

## 6 Conclusion

We address the issue that rough/incomplete boundaries in segmenting 3D-GS and propose a novel Boundary-enhanced segmentation pipeline. Given input

prompts on the first rendering view, our approach automatically generates multi-view masks and achieves consistent 3D segmentation via the proposed assignment strategy. Our Gaussian Decomposition module can effectively mitigate the boundary roughness issue of segmented objects resulting from the inherent geometry structure in 3D-GS. Extensive segmentation experiments show that our method can effectively obtain high-quality 3D object segmentation without boundary issues, and different scene-editing tasks demonstrate that our method can be easily applied to downstream applications. Overall, we hope our work can inspire more future work in the area of 3D Gaussian representation.

## References

1. Barber, C.B., Dobkin, D.P., Huhdanpaa, H.: The quickhull algorithm for convex hulls. *ACM Transactions on Mathematical Software (TOMS)* **22**(4), 469–483 (1996) [12](#)
2. Barron, J.T., Mildenhall, B., Verbin, D., Srinivasan, P.P., Hedman, P.: Mipnerf 360: Unbounded anti-aliased neural radiance fields. In: *Proceedings of the IEEE/CVF Conference on Computer Vision and Pattern Recognition*. pp. 5470–5479 (2022) [8](#), [10](#), [11](#)
3. Cen, J., Fang, J., Yang, C., Xie, L., Zhang, X., Shen, W., Tian, Q.: Segment any 3d gaussians. *arXiv preprint arXiv:2312.00860* (2023) [2](#), [4](#), [8](#), [9](#), [10](#)
4. Cen, J., Zhou, Z., Fang, J., Shen, W., Xie, L., Zhang, X., Tian, Q.: Segment anything in 3d with nerfs. *arXiv preprint arXiv:2304.12308* (2023) [4](#), [8](#), [9](#), [10](#)
5. Chen, A., Xu, Z., Geiger, A., Yu, J., Su, H.: Tensorf: Tensorial radiance fields. In: *Proc. ECCV*. pp. 333–350. Springer (2022) [1](#)
6. Chen, Z., Wang, F., Liu, H.: Text-to-3d using gaussian splatting. *arXiv preprint arXiv:2309.16585* (2023) [3](#)
7. Fan, L., Wang, F., Wang, N., ZHANG, Z.X.: Fully sparse 3d object detection. *Advances in Neural Information Processing Systems* **35**, 351–363 (2022) [1](#)
8. Fan, L., Xiong, X., Wang, F., Wang, N., Zhang, Z.: Rangedet: In defense of range view for lidar-based 3d object detection. In: *Proc. ICCV*. pp. 2918–2927 (2021) [1](#)
9. Goel, R., Sirikonda, D., Saini, S., Narayanan, P.: Interactive segmentation of radiance fields. In: *Proceedings of the IEEE/CVF Conference on Computer Vision and Pattern Recognition*. pp. 4201–4211 (2023) [4](#)
10. Hu, Q., Yang, B., Khalid, S., Xiao, W., Trigoni, N., Markham, A.: Towards semantic segmentation of urban-scale 3d point clouds: A dataset, benchmarks and challenges. In: *Proc. CVPR*. pp. 4977–4987 (2021) [1](#)
11. Jin, H., Liu, I., Xu, P., Zhang, X., Han, S., Bi, S., Zhou, X., Xu, Z., Su, H.: Tensorf: Tensorial inverse rendering. In: *Proc. CVPR*. pp. 165–174 (2023) [1](#)
12. Kerbl, B., Kopanas, G., Leimkühler, T., Drettakis, G.: 3d gaussian splatting for real-time radiance field rendering. *ACM Transactions on Graphics* **42**(4), 1–14 (2023) [2](#), [3](#), [5](#), [8](#)
13. Kerr, J., Kim, C.M., Goldberg, K., Kanazawa, A., Tancik, M.: LERF: Language embedded radiance fields. In: *Proceedings of the IEEE/CVF International Conference on Computer Vision*. pp. 19729–19739 (2023) [4](#), [8](#), [10](#)
14. Kirillov, A., Mintun, E., Ravi, N., Mao, H., Rolland, C., Gustafson, L., Xiao, T., Whitehead, S., Berg, A.C., Lo, W.Y., et al.: Segment anything. *arXiv preprint arXiv:2304.02643* (2023) [3](#)
15. Lai, X., Liu, J., Jiang, L., Wang, L., Zhao, H., Liu, S., Qi, X., Jia, J.: Stratified transformer for 3d point cloud segmentation. In: *Proc. CVPR*. pp. 8500–8509 (2022) [1](#)
16. Lan, K., Li, H., Shi, H., Wu, W., Liao, Y., Wang, L., Zhou, P.: 2d-guided 3d gaussian segmentation. *arXiv preprint arXiv:2312.16047* (2023) [2](#), [4](#)
17. Li, Z., Wang, W., Li, H., Xie, E., Sima, C., Lu, T., Qiao, Y., Dai, J.: Bevformer: Learning bird’s-eye-view representation from multi-camera images via spatiotemporal transformers. In: *Proc. ECCV*. pp. 1–18. Springer (2022) [2](#)
18. Liu, S., Zeng, Z., Ren, T., Li, F., Zhang, H., Yang, J., Li, C., Yang, J., Su, H., Zhu, J., et al.: Grounding dino: Marrying dino with grounded pre-training for open-set object detection. *arXiv preprint arXiv:2303.05499* (2023) [9](#)

19. Luiten, J., Kopanas, G., Leibe, B., Ramanan, D.: Dynamic 3d gaussians: Tracking by persistent dynamic view synthesis. arXiv preprint arXiv:2308.09713 (2023) **3**
20. Meyer, G.P., Laddha, A., Kee, E., Vallespi-Gonzalez, C., Wellington, C.K.: Laser-net: An efficient probabilistic 3d object detector for autonomous driving. In: Proc. CVPR. pp. 12677–12686 (2019) **1**
21. Mildenhall, B., Srinivasan, P., Tancik, M., Barron, J., Ramamoorthi, R., Ng, R.: Nerf: Representing scenes as neural radiance fields for view synthesis. In: Proc. ECCV (2020) **1**
22. Mildenhall, B., Srinivasan, P.P., Ortiz-Cayon, R., Kalantari, N.K., Ramamoorthi, R., Ng, R., Kar, A.: Local light field fusion: Practical view synthesis with prescriptive sampling guidelines. ACM Transactions on Graphics (TOG) **38**(4), 1–14 (2019) **8, 14**
23. Mirzaei, A., Aumentado-Armstrong, T., Derpanis, K.G., Kelly, J., Brubaker, M.A., Gilitshenski, I., Levinshtein, A.: Spin-nerf: Multiview segmentation and perceptual inpainting with neural radiance fields. In: Proceedings of the IEEE/CVF Conference on Computer Vision and Pattern Recognition. pp. 20669–20679 (2023) **8, 9, 10**
24. Ng, M.H., Radia, K., Chen, J., Wang, D., Gog, I., Gonzalez, J.E.: Bev-seg: Bird’s eye view semantic segmentation using geometry and semantic point cloud. arXiv preprint arXiv:2006.11436 (2020) **2**
25. Pan, C., He, Y., Peng, J., Zhang, Q., Sui, W., Zhang, Z.: Baeformer: Bi-directional and early interaction transformers for bird’s eye view semantic segmentation. In: Proc. CVPR. pp. 9590–9599 (2023) **2**
26. Pan, X., Xia, Z., Song, S., Li, L.E., Huang, G.: 3d object detection with point-former. In: Proc. CVPR. pp. 7463–7472 (2021) **1**
27. Peng, L., Chen, Z., Fu, Z., Liang, P., Cheng, E.: Bevsegformer: Bird’s eye view semantic segmentation from arbitrary camera rigs. In: Proc. WACV. pp. 5935–5943 (2023) **2**
28. Ren, Z., Agarwala, A., Russell, B., Schwing, A.G., Wang, O.: Neural volumetric object selection. In: Proceedings of the IEEE/CVF Conference on Computer Vision and Pattern Recognition. pp. 6133–6142 (2022) **4**
29. Shi, S., Wang, X., Li, H.: Pointcnn: 3d object proposal generation and detection from point cloud. In: Proc. CVPR. pp. 770–779 (2019) **1**
30. Sun, C., Sun, M., Chen, H.T.: Direct voxel grid optimization: Super-fast convergence for radiance fields reconstruction. In: Proc. CVPR. pp. 5459–5469 (2022) **1**
31. Tang, J., Ren, J., Zhou, H., Liu, Z., Zeng, G.: Dreamgaussian: Generative gaussian splatting for efficient 3d content creation. arXiv preprint arXiv:2309.16653 (2023) **3**
32. Tschernezki, V., Laina, I., Larlus, D., Vedaldi, A.: Neural feature fusion fields: 3d distillation of self-supervised 2d image representations. In: 2022 International Conference on 3D Vision (3DV). pp. 443–453. IEEE (2022) **4**
33. Yang, C., Chen, Y., Tian, H., Tao, C., Zhu, X., Zhang, Z., Huang, G., Li, H., Qiao, Y., Lu, L., et al.: Bevformer v2: Adapting modern image backbones to bird’s-eye-view recognition via perspective supervision. In: Proc. CVPR. pp. 17830–17839 (2023) **2**
34. Ye, M., Danelljan, M., Yu, F., Ke, L.: Gaussian grouping: Segment and edit anything in 3d scenes. arXiv preprint arXiv:2312.00732 (2023) **2, 4**
35. Yi, T., Fang, J., Wu, G., Xie, L., Zhang, X., Liu, W., Tian, Q., Wang, X.: Gaussiandreamer: Fast generation from text to 3d gaussian splatting with point cloud priors. arXiv preprint arXiv:2310.08529 (2023) **3**

36. Zhi, S., Laidlow, T., Leutenegger, S., Davison, A.J.: In-place scene labelling and understanding with implicit scene representation. In: Proceedings of the IEEE/CVF International Conference on Computer Vision. pp. 15838–15847 (2021) [4](#)
37. Zhou, S., Chang, H., Jiang, S., Fan, Z., Zhu, Z., Xu, D., Chari, P., You, S., Wang, Z., Kadambi, A.: Feature 3dgs: Supercharging 3d gaussian splatting to enable distilled feature fields. arXiv preprint arXiv:2312.03203 (2023) [2](#), [4](#)
38. Zwicker, M., Pfister, H., Van Baar, J., Gross, M.: Ewa volume splatting. In: Proceedings Visualization, 2001. VIS'01. pp. 29–538. IEEE (2001) [7](#)